Avoiding Volumetric Locking in Ten-Node Tetrahedral Finite Elements for Explicit Finite Element Simulations

Tolga Usta[1], Malte von Scheven[1], Manfred Bischoff[1]

[1] University of Stuttgart, Institute for Structural Mechanics
Pfaffenwaldring 7, 70569 Stuttgart, Germany

1 Abstract

Simulations involving nearly incompressible materials require particular attention during the setup phase, as volumetric locking phenomena might significantly distort the results. Researchers have proposed various methods to address this issue. One widely adopted technique for eight-node hexahedral solid elements is to combine reduced-order integration with hourglass stabilization. However, this method relies on a mesh composed of hexahedral elements, which for complex structures often cannot be achieved. Complex structures typically require tetrahedral elements to ensure an accurate representation, and automated meshing algorithms tend to generate meshes dominated by tetrahedral elements for such structures. Therefore, removing volumetric locking for tetrahedral elements is especially important.

This work revisits the method proposed by Lo and Ling [1], which decomposes the element stiffness matrix into a constant and a higher-order part. Preserving the constant part ensures element consistency, while the higher-order part is specifically treated using a modified value for the bulk modulus. This modification directly targets the root cause of the unwanted volumetric locking. The proposed approach is extended to support explicit time integration schemes and it is integrated into LS-DYNA for ten-node tetrahedral elements with five integration points as a user-defined isotropic linear elastic material model. A series of numerical simulations validates the effectiveness of the proposed method.

Keywords: finite element technology, volumetric locking, tetrahedral solid element

2 Introduction

The objective of the finite element method is to achieve an accurate solution while minimizing the total time required to obtain results, including pre-processing time, simulation time and post-processing time. Engineers usually employ automated mesh generation algorithm, which reduces the pre-processing time significantly. The mesh generation process may be seen trivial for geometrically rather simple structures; but it is a challenging task for structures with complex geometrical features. To overcome this challenge, many automated mesh generation algorithms often employ tetrahedral finite elements, resulting in tetrahedral element dominated meshes. Nevertheless, engineers prefer hexahedral element dominant meshes for sophisticated simulation models [2] over tetrahedral dominated ones, since hexahedral elements yield more accurate results in general for a rather small computational cost increase.

As an example, consider a 1x1x1 incompressible rubber-cube discretized using one single eight-node hexahedral element with linear shape functions. The element has a constant Jacobian matrix. Using the Gaussian quadrature method, eight Gauss points are necessary for an exact integration of the element stiffness matrix numerically. This numerical scheme is referred to as *full integration*. In the near incompressible limit, where the material property bulk modulus tends to infinity ($K \to \infty$), *a full integration method* captures the correct isochoric behavior; but, yields very high stiffness for any volume changing deformation. This phenomenon is called as the volumetric locking. In this case, using a *reduced integration method* with an hourglass stabilization is one of the well-known methods to remove volumetric locking for hexahedral element formulations [3]. The reduced integration method relaxes the element stiffness by using fewer integration points than a full integration method, which results in zero-energy modes as a consequence. By introducing an hourglass stabilization, these zero-energy modes are suppressed, and the element stress response is kept within a physically reasonable limit. Besides the advantages of a hexahedral-dominated mesh, it is still a complicated task to create hexahedral dominated

meshes for geometrically complex structures. In many cases, the process requires know-how. Therefore, addressing the volumetric locking problem is essential in the tetrahedral element family.

Considering the four-node tetrahedral element with displacement degrees of freedom, due to mathematical and inherent geometrical constraints, there is virtually no option to remove the locking effects on element level. As a result, the element is prone to both shear and volumetric locking. To enhance the accuracy of the four-node tetrahedral element, various approaches have been proposed. For example, the introduction of additional rotational degrees of freedom was proposed in [4], which significantly improves the element performance in case of shear locking. Bonet and Burton [5] proposed an average nodal pressure tetrahedron, which alleviates volumetric locking at the patch level. Nevertheless, the four-node tetrahedral element generally remains too stiff, and its simulation results are less accurate than those obtained with eight-node hexahedral or ten-node tetrahedral elements.

The ten-node tetrahedral element formulation, in contrast, does not suffer from shear locking, as the displacement field is approximated with quadratic shape functions over the element domain. However, volumetric locking remains a challenge. In [6], a ten-node tetrahedral element composed of twelve four-node tetrahedra was proposed. This approach assumes a linear deformation in the element domain and four volume constraints per element are introduced. Nevertheless, numerical results indicate that the accuracy of this formulation deteriorates in the near-incompressible limit. A similar approach was presented in [7], where the ten-node element is treated as a collection of eight four-node tetrahedra. In this method, the strain field is first approximated using a mean-strain strain-displacement operator, which is subsequently corrected through an energy-sampling technique. Another line of work is the Cosserat point element formulation for ten-node tetrahedra [8]. Here, the deformation modes of the element are modeled via a strain energy function based on the hyperelastic constitutive equations of the Cosserat point element. This approach was later extended to general hypoelastic material models, while keeping the hourglass stabilization unchanged, and subsequently implemented in LS-DYNA [9]. Despite these advances, the ten-node tetrahedral Cosserat point element is significantly more computationally expensive than the standard ten-node tetrahedral element. Lo and Ling [1] proposed yet another strategy, in which the element stiffness matrix is split into a constant and a higher-order part. In the near-incompressible limit, the compatibility condition for the constant strain part is relaxed and the incompressibility condition is introduced to the higher-order part.

In this work, we revisit the method in [1]. Similarly, the element stiffness matrix is split into constant and higher-order parts. We extend this formulation to an explicit time-integration scheme under the assumption of isotropic linear elasticity for small deformations. The extended formulation is integrated into LS-DYNA for ten-node tetrahedral elements with five integration points as a user-defined isotropic linear elastic material model. Finally, a series of numerical examples is presented, comparing the standard ten-node tetrahedra, the ten-node Cosserat point tetrahedra and the proposed modified ten-node tetrahedra element formulations.

3 Tetrahedral Element Family

Tetrahedral elements are the simplest three-dimensional solid elements in the finite element method. The most basic member of this family is the four-node tetrahedral element, which consists of four triangular faces and has nodes located at each corner. The element domain is represented using linear shape functions, meaning that the displacement field is approximated linearly within the element. Consequently, this element can only represent a constant strain state, requiring only a single integration point for numerical integration. The four-node tetrahedral element is quite economic and it is well-suited to generate meshes for complex structures. However, due to mathematical reasons and inherent geometric constraints, the four-node tetrahedral element with only nodal displacement degrees of freedom is highly prone to locking, namely, shear locking and volumetric locking. Moreover, there is essentially no possibility of eliminating these locking effects at the element level.

To illustrate the inherent geometric constraints, consider a three-dimensional Cartesian coordinate system in which that any node located on the xy-, yz- and xz-planes (i.e., coordinate planes) is assumed to be fixed in all three displacement degrees of freedom. Now, place a single four-node tetrahedral element in this space such that three nodes lie on the xy-plane, as shown in Figure 1(a). The fourth node, $\boldsymbol{P}$, is not located on any coordinate plane and can therefore move freely parallel to the xy-plane, allowing an isochoric (volume-preserving) deformation, i.e., a purely shape-changing deformation. Next, introduce

a second four-node tetrahedral element, with three of its nodes lying on the xz-plane and the fourth node coinciding with the node $\boldsymbol{P}$, as illustrated in Figure 1(b). In this configuration, the node $\boldsymbol{P}$ can no longer move in y-direction, since such a displacement would violate the isochoric deformation condition of the second tetrahedra. Finally, introduce a third tetrahedral element, with three of its nodes are on the yz-plane and again the fourth node coinciding with the node $\boldsymbol{P}$, as shown in Figure 1(c). At this point, an isochoric deformation of the system is no longer possible: all displacement degrees of freedom of the node $\boldsymbol{P}$ are implicitly constrained, leading to locking.

Ten-node tetrahedral elements, in contrast, include additional six nodes located at the midpoints of each edge. These additional 18 degrees of freedom relax the inherent geometrical constraints and help to remove shear locking. Since the volumetric locking is purely associated with the material property, namely the bulk modulus K, the element still suffers from volumetric locking, particularly in the nearly incompressible regime. The displacement field is interpolated using quadratic shape functions, which require four integration points for exact numerical integration of the stiffness matrix. As with the four-node family member, ten-node tetrahedral elements are also well-suited for meshing complex geometries. Moreover, an existing four-node tetrahedral element mesh can be transformed into the ten-node tetrahedral element mesh simply by inserting mid-edge nodes. Overall, this element formulation provides a significantly improved accuracy, albeit at an increased computational cost.

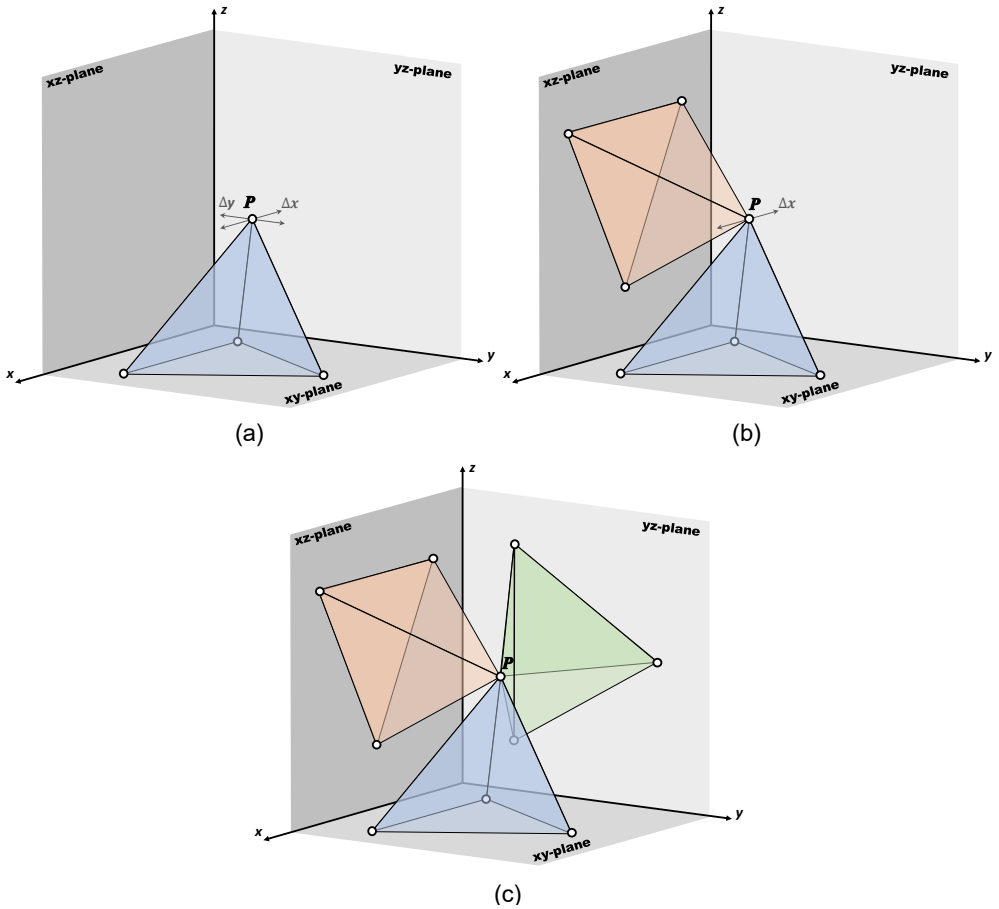

Fig.1: Illustration of inherent geometrical constraints of four-node tetrahedral elements, shown using volume preserving displacements of node $\boldsymbol{P}$ under various cases. All nodes lying on the coordinate planes are assumed to be fixed.

Cubic and other higher-order tetrahedral elements have also been proposed in the literature. Since these formulations are beyond the scope of this work, we refer the interested reader to the relevant studies [10,15]. It is worth noting that the fundamental starting point for constructing finite elements in any dimension can be the Pascal's triangle, which provides a systematic way to determine the span of shape functions in multiple dimensions. A detailed presentation of tetrahedral shape functions up to cubic order, together with their representation on Pascal's triangle, can be found in [10], therefore, they are omitted in this work.

4 Modified Ten-Node Tetrahedral Element Formulation

4.1 Modified Element Stiffness Matrix

The root cause of the volumetric locking is material incompressibility, which is directly related to the bulk modulus of the material. Consider the isotropic linear elastic material matrix $\boldsymbol{C}$ given as,

$$\boldsymbol{C} = \begin{bmatrix} K+\frac{4G}{3} & K-\frac{2G}{3} & K-\frac{2G}{3} & 0 & 0 & 0 \\ K-\frac{2G}{3} & K+\frac{4G}{3} & K-\frac{2G}{3} & 0 & 0 & 0 \\ K-\frac{2G}{3} & K-\frac{2G}{3} & K+\frac{4G}{3} & 0 & 0 & 0 \\ 0 & 0 & 0 & G & 0 & 0 \\ 0 & 0 & 0 & 0 & G & 0 \\ 0 & 0 & 0 & 0 & 0 & G \end{bmatrix} \text{ with } \begin{matrix} K = \frac{E}{3(1-2\nu)} \\ G = \frac{E}{2(1+\nu)} \end{matrix} \quad (1)$$

In the near-incompressible limit, i.e., $\nu \to 0.5$, the bulk modulus tends to infinity ($K \to \infty$). The element stiffness matrix $\boldsymbol{k}$, computed using the strain-displacement matrix $\boldsymbol{\mathcal{B}}$ and the material matrix $\boldsymbol{C}$, therefore exhibits an excessively stiff response, especially for volume-changing deformations. As a result, for any strain tensor $\boldsymbol{\varepsilon}$ with $tr(\boldsymbol{\varepsilon}) \neq 0$, unphysically large stress responses are obtained. To remove the volumetric locking, the modified ten-node tetrahedral element formulation splits the element stiffness matrix into a constant and a higher-order part. The constant part is preserved to maintain element consistency, while the higher-order part is modified to remove volumetric locking. Consider the standard element stiffness matrix $\boldsymbol{k}$ of the standard ten-node tetrahedral element given as,

$$\boldsymbol{k} = \int_{V_e} \boldsymbol{\mathcal{B}}^T \boldsymbol{C} \boldsymbol{\mathcal{B}} dV \quad (2)$$

Similarly, $\boldsymbol{k^0}$ can be defined as,

$$\boldsymbol{k^0} = \int_{V_e} \boldsymbol{\mathcal{B}}^T \boldsymbol{C}^0 \boldsymbol{\mathcal{B}} dV \quad (3)$$

where the material matrix $\boldsymbol{C}^0$ is computed using a modified Poisson's ratio of $\nu = 0$. Accordingly, $\boldsymbol{k}$ and $\boldsymbol{k^0}$ are split into a constant and a higher-order part as,

$$\begin{aligned} \boldsymbol{k} &= \boldsymbol{k_c} + \boldsymbol{k_h} \\ \boldsymbol{k^0} &= \boldsymbol{k_c^0} + \boldsymbol{k_h^0} \end{aligned} \quad (4)$$

Here, the subscripts $\boldsymbol{c}$ and $\boldsymbol{h}$ refer to constant and higher-order parts, respectively. By Substituting $\boldsymbol{k_h}$ with $\boldsymbol{k_h^0}$, the modified element stiffness matrix $\bar{\boldsymbol{k}}$ for the modified ten-node tetrahedral element is defined as,

$$\begin{aligned} \bar{\boldsymbol{k}} &= \boldsymbol{k_c} + \boldsymbol{k_h^0} \\ &= \boldsymbol{k_c} + (\boldsymbol{k^0} - \boldsymbol{k_c^0}) \\ &= (\boldsymbol{k_c} - \boldsymbol{k_c^0}) + \boldsymbol{k^0} \end{aligned} \quad (5)$$

Since the constant part is valid throughout the element domain, it is evaluated at the element center. By introducing the isoparametric concept and evaluating the modified element stiffness matrix $\bar{\boldsymbol{k}}$ numerically, Equation (5) yields,

$$\bar{\boldsymbol{k}} = \underbrace{(\boldsymbol{\mathcal{B}}^T(\boldsymbol{C} - \boldsymbol{C}^0)\boldsymbol{\mathcal{B}}|\boldsymbol{J}|w)_{\xi_c}}_{\boldsymbol{k_c} - \boldsymbol{k_c^0}} + \underbrace{\sum_{i=1}^{n_{GP}} \boldsymbol{\mathcal{B}}_i^T \boldsymbol{C}^0 \boldsymbol{\mathcal{B}}_i |\boldsymbol{J}_i| w_i}_{\boldsymbol{k^0}} \quad (6)$$

where $\boldsymbol{\mathcal{B}}$ denotes the strain-displacement matrix, w the weighting factor, $\boldsymbol{J}$ the Jacobian matrix, $|\boldsymbol{J}|$ its determinant and $\boldsymbol{\xi_c}$ the center integration point. The subscript i indicates that the corresponding variable is evaluated at the i^{th} integration point. As can be seen in Equation (6), $\boldsymbol{k_c}$ and $\boldsymbol{k_c^0}$ are evaluated at the element center, while $\boldsymbol{k^0}$ is evaluated using the standard quadrature rule.

The integration point coordinates of the isoparametric ten-node tetrahedral element with four integration points and an additional center integration point, together with the corresponding weighting factors, are listed in Table 1. If only the center integration point and the first term of the Equation (6) are considered, the element stiffness matrix exhibits zero-energy modes. Introducing the off-center integration points, as in the second term of the Equation (6), stabilizes these modes. Therefore, the proposed modified

ten-node tetrahedral element formulation aligns with Borrvall's description of the Cosserat point element formulations in LS-DYNA, "Reduced *integrated* element with stabilization, even for the high-order tetrahedron." [9].

Table 1: Integration point positions for the isoparametric modified ten-node tetrahedral element with four integration points and an additional center integration point

Integration Point	ξ	η	ζ	w
1	0.138	0.138	0.138	0.25
2	0.138	0.585	0.585	0.25
3	0.585	0.138	0.585	0.25
4	0.585	0.585	0.138	0.25
Center	0.25	0.25	0.25	1.0

4.2 Modified Stress Post-Processing and Extension of the Method for Explicit Time Integration Scheme

Similar to the computation of the modified element stiffness matrix, corresponding modifications are applied to the stress post-processing. Using the numerically computed field variables, the modified stress vector $\bar{\boldsymbol{\sigma}}_i$ at the i^{th} integration point in Voigt notation can be computed as,

$$\begin{aligned}\bar{\boldsymbol{\sigma}}_i &= (\boldsymbol{\sigma}_c - \boldsymbol{\sigma}_c^0) + \boldsymbol{\sigma}_i^0 \\ &= [(\boldsymbol{C} - \boldsymbol{C}^0)\boldsymbol{\mathcal{B}}\boldsymbol{d}]_{\xi_c} + (\boldsymbol{C}^0\boldsymbol{\mathcal{B}}\boldsymbol{d})_{\xi_i} \\ &= \underbrace{[(\boldsymbol{C} - \boldsymbol{C}^0)\boldsymbol{\varepsilon}]_{\xi_c}}_{\boldsymbol{\sigma}_c - \boldsymbol{\sigma}_c^0} + \underbrace{(\boldsymbol{C}^0\boldsymbol{\varepsilon})_{\xi_i}}_{\boldsymbol{\sigma}_i^0}\end{aligned} \tag{7}$$

Subsequently, the modified ten-node tetrahedral element formulation can be simplified for the explicit time integration scheme, since explicit analysis does not require computation of the element stiffness matrix. Instead, the internal force vector of the element must be computed. Assuming the element strain vector $\boldsymbol{\varepsilon}^{\boldsymbol{\tau}}(\xi, \eta, \zeta)$ in Voigt notation at the time τ is known, the stress vector $\bar{\boldsymbol{\sigma}}_i^{\tau}$ at the i^{th} integration can be computed using Equation (7) as,

$$\bar{\boldsymbol{\sigma}}_i^{\tau} = \underbrace{[(\boldsymbol{C} - \boldsymbol{C}^0)\boldsymbol{\varepsilon}^{\tau}]_{\xi_c}}_{\boldsymbol{\sigma}_c{}^{\tau} - \boldsymbol{\sigma}_c^{0\,\tau}} + \underbrace{(\boldsymbol{C}^0\boldsymbol{\varepsilon}^{\tau})_{\xi_i}}_{\boldsymbol{\sigma}_i^{0\,\tau}} \tag{8}$$

Then, for the isoparametric ten-node tetrahedral element with four integration points and an additional center integration point, the internal force vector of the element at the time τ is computed as,

$$\bar{\boldsymbol{f}}_{int}^{\tau} = (\boldsymbol{\mathcal{B}}_c^{\boldsymbol{T}}(\boldsymbol{\sigma}_c{}^{\tau} - \boldsymbol{\sigma}_c^{0\,\tau})|\boldsymbol{J}_c|w_c) + \sum_{i=1}^{4}(\boldsymbol{\mathcal{B}}_i^{\boldsymbol{T}}\boldsymbol{\sigma}_i^{0\,\tau}|\boldsymbol{J}_i|w_i) \tag{9}$$

where the subscript c indicates that the corresponding variable is evaluated at the center integration point.

Using the modified internal force vector, the time-step update is performed in the standard manner of the explicit integration scheme. Specifically, the nodal accelerations are first obtained from the balance of internal and external forces, followed by the velocity and displacement updates at each time step. In this way, the incorporation of the modified formulation does not alter the fundamental structure of the explicit algorithm; it only affects the evaluation of the internal forces, ensuring that the element response remains free from volumetric locking.

4.3 Modified Ten-Node Tetrahedral Element Implementation using LS-DYNA User Interface

The modified ten-node tetrahedral element formulation requires access to element-level data such as the strain-displacement matrix and the integration point positions. Therefore, implementing the modified formulation as a user-element is necessary to access these data directly. However, the current LS-DYNA user-element interface supports elements up to eight nodes. Consequently, an implementation of a modified ten-node tetrahedral element as a user-element is not possible.

As an alternative, the standard implementation of the ten-node tetrahedral element with five integration points can be employed in combination with the user-defined materials interface. The integration point positions and corresponding weighting factors for this element are listed in Table 2.

Table 2: Integration point positions for the isoparametric ten-node tetrahedral element with five integration points

Integration Point	ξ	η	ζ	w
1	0.25	0.25	0.25	-0.8
2	0.5	0.1667	0.1667	0.45
3	0.1667	0.5	0.1667	0.45
4	0.585	0.138	0.585	0.45
5	0.585	0.585	0.138	0.45

As shown in Table 2, the first integration point is located at the element center, which can be used for the modified ten-node tetrahedral element formulation described in the previous section. All five integration points are used to compute the higher-order term of Equation (8), while only the center integration point is used to evaluate the constant term of Equation (8). Consequently, the material routine is modified for the first integration point, so that the material model equations are computed once with the modified Poisson's ratio and once with the correct Poisson's ratio during the iteration over integration points. The constant term of Equation (8) is then stored as history variables, which can be accessed via the user-material interface and subsequently used for stress post-processing at the remaining integration points. After computing the stress state at all integration points, the internal force vector is obtained as given in Equation (9).

However, an inconsistency arises regarding the weighting factor of the first integration point. As discussed earlier, the constant term is valid for the entire element domain, which implies that its weighting factor should be equal to unity in the internal force computation. In the standard implementation of the ten-node tetrahedral element with five integration points, however, the weighting factors of the integration points cannot be directly accessed through user-defined materials interface. To overcome this limitation, the constant term of Equation (9) is scaled by a correction factor such that the effective weighting factor becomes unity for the internal force vector computation. This work-around ultimately yields a modified version of Equation (9), given as,

$$\bar{\boldsymbol{f}}_{int}^{\tau} = (\boldsymbol{\mathcal{B}}_{\mathbf{1}}^{\boldsymbol{T}}(\boldsymbol{\sigma}_1{}^{\tau} - \boldsymbol{\sigma}_1^{0^{\tau}})|\boldsymbol{J}_1|w_1)w_{cor} + \sum_{i=1}^{5}(\boldsymbol{\mathcal{B}}_i^{\boldsymbol{T}}\boldsymbol{\sigma}_i^{0^{\tau}}|\boldsymbol{J}_i|w_i) \quad with \quad w_{cor} = {}^{-10}/_{8} \tag{10}$$

Similarly, the stress post-processing follows an analogous modification strategy. In particular, the stress evaluation at each integration point is carried out using the procedure outlined previously. The stresses computed at the center integration point using the modified Poisson's ratio and the correct value, which provide the basis for separating the constant and higher-order contributions. These quantities are then stored as history variables and they are made available for all off-center integration points. Accordingly, the modified stress post-processing takes the form,

$$\bar{\boldsymbol{\sigma}}_i^{\tau} = \underbrace{[(\boldsymbol{C} - \boldsymbol{C}^0)\boldsymbol{\varepsilon}^{\tau}]_{\xi_1}}_{\boldsymbol{\sigma}_1{}^{\tau} - \boldsymbol{\sigma}_1^{0^{\tau}}} + \underbrace{\boldsymbol{C}^0\boldsymbol{\varepsilon}_i^{\tau}}_{\boldsymbol{\sigma}_i^{0^{\tau}}} \tag{11}$$

5 Numerical Examples

Various numerical examples are presented in this section to demonstrate the modified ten-node tetrahedral element formulation for an isotropic linear elastic material model. The LS-DYNA user-interface implementation, which was described in the previous section, was used for all examples. The user-defined material card for the numerical examples is given in Table 3.

*Table 3: Material card ***MAT_USER_DEFINED_MATERIAL_MODELS** for numerical examples*

MID	**RO**	**MT**	**LMC**	**NHV**	**IORTHO**	**IBULK**	**IG**
1	7.85E-6	41	4	29	0	3	4
IVECT	**IFAIL**	**ITHERM**	**IHYPER**	**IEOS**	**LMCA**		
0	0	0	0	0	0		

P1	P2	P3	P4				
&emod	&possrat	&bulk	&gmod				

Bulk modulus (&bulk) and shear modulus (&gmod) were computed directly using specified Young's modulus (&emod) and Poisson's ratio (&possrat) via Equation (12) and Equation (13), respectively.

$$K = \frac{E}{3(1-2\nu)} \tag{12}$$

$$G = \frac{E}{2(1+\nu)} \tag{13}$$

Unless otherwise specified, all numerical examples were conducted using material properties of an almost incompressible solid, with a Young's modulus of $E = 207$ and a Poisson's ratio of $\nu = 0.4999$.

5.1 Patch Test for Explicit Time Integration

A patch test for explicit time integration scheme according to [11] was employed to investigate the consistency of the proposed element formulation. Figure 2 illustrates the two meshes used for the patch test. A linear initial velocity field, $v(x) = 0.02 \cdot x$, was prescribed in the x-direction on nodes, which results in a constant strain state in the domain. Under these conditions, all elements in the patch produced the same constant stress state, thereby validating the proposed formulation.

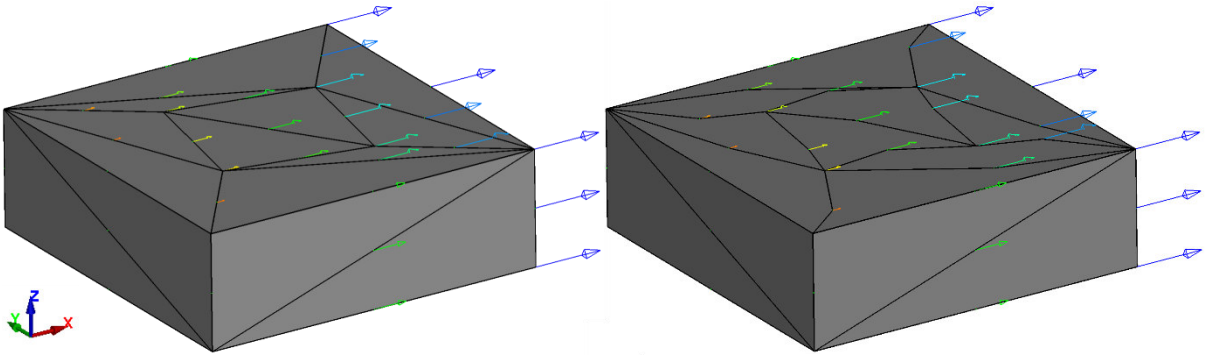

Fig.2: Straight-edge ten-node tetrahedral element mesh (left) and curved-edge ten-node tetrahedral element mesh (right) used for the patch test in explicit time integration. Initial nodal velocities are shown as vectors.

5.2 Cylindrical Pressure Vessel

This well-known small-deformations benchmark problem considers a cylindrical pressure vessel, with both ends clamped, subjected to internal and external pressure loading [12]. A cylindrical section of the vessel, illustrated in Figure 3(left), was taken sufficiently far from the ends, and body forces were neglected, so that plane strain conditions apply. To reduce computational cost, only a quarter of this section was modeled using the finite element method. The objective is to investigate the performance of various discretizations under nearly incompressible material behavior.

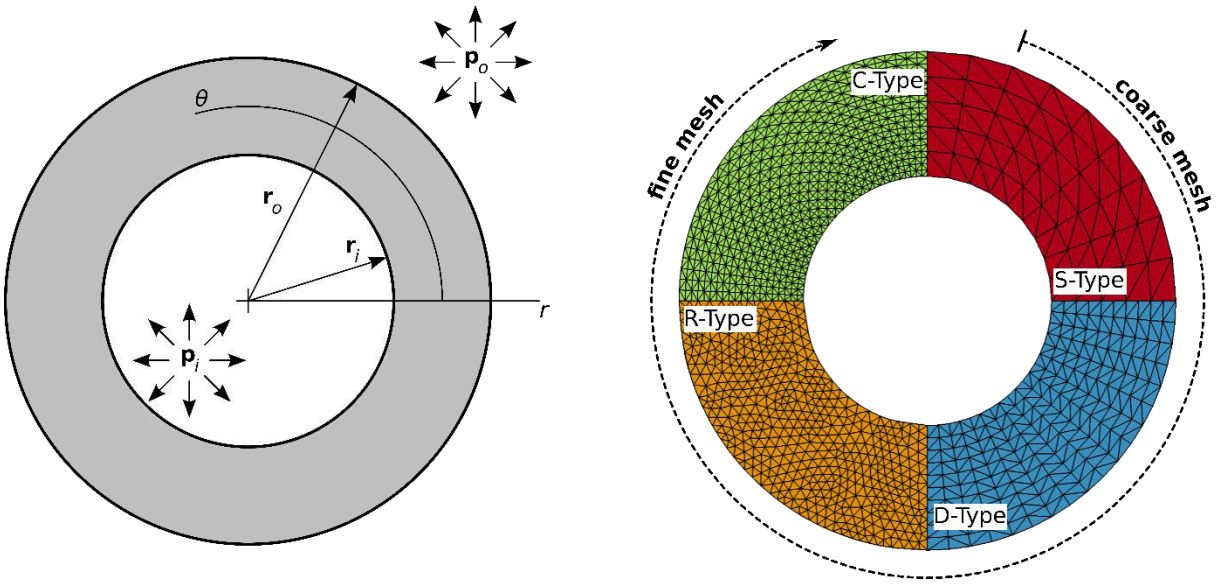

Fig.3: The cross-section of the cylindrical pressure vessel (left) and representative examples of the used finite element discretizations (right)

The finest mesh used in the simulations consists of 41,769 degrees of freedom, corresponding to an average characteristic element length of approximately 0.13. In contrast, the coarsest mesh contains only 1,881 degrees of freedom with an average characteristic element length of about 0.67. Four different discretization strategies were employed: the rotationally symmetric single-element-row mesh (S-Type), the rotationally symmetric double-element-row mesh (D-Type), the rotationally symmetric crossed-element-row mesh (C-Type), and the random mesh (R-Type). Representative examples of these discretizations are illustrated in Figure 3(right).

The benchmark problem is modeled as an explicit quasi-static analysis. The simulations were carried out using three different tetrahedral element formulations: the standard ten-node tetrahedral element, the ten-node Cosserat point tetrahedral element, and the modified ten-node tetrahedral element. Rather than directly comparing the full stress state of the solutions, the stress triaxiality, η, was compared. This scalar quantity is defined as the ratio of the mean stress to the equivalent von Mises stress, as expressed in Equation (14). Stress triaxiality is widely used in fracture mechanics as an indicator of fracture type, distinguishing between ductile and brittle failure mechanisms.

$$\eta = \frac{\frac{1}{3}(\sigma_{11}+\sigma_{22}+\sigma_{33})}{\sqrt{\frac{(\sigma_{11}-\sigma_{22})^2+(\sigma_{22}-\sigma_{33})^2+(\sigma_{33}-\sigma_{11})^2+6(\sigma_{12}^2+\sigma_{23}^2+\sigma_{31}^2)}{2}}} \tag{14}$$

In addition, the stress triaxiality of the finite element solutions in the radial direction was evaluated and compared with the analytical reference solution. The latter can be derived from the closed-form expression of the stress state presented in [12]. For the parameters $E = 207$, $r_i = 5$, $r_o = 10$, $p_i = 0.00207$ and $p_o = 0.0$, the analytical stress triaxiality can be computed as,

$$\eta(r,\nu) = \frac{4.6\cdot10^{-4}(1+\nu)}{\sqrt{\frac{1.4283\cdot10^{-2}}{r^4}+4.761\cdot10^{-7}-1.9044\cdot10^{-6}(1-\nu)\nu}} \tag{15}$$

Comparison plots of the three element formulations using different discretizations are shown in Figure 4. The stress triaxiality results of the finite element simulations were evaluated along an element column selected in the radial direction, where the averaged stress triaxiality of elements were considered for the relative L^2-error norm computation. The vertical axis represents the relative L^2-error norm of the stress triaxiality with respect to the analytical solution, while the horizontal axis shows the total number of degrees of freedom of the FE discretization. The results indicate that the overall accuracy of the Cosserat point and the modified formulations is satisfactory for all discretizations. In contrast, the standard ten-node tetrahedral element exhibits poor accuracy for S-Type mesh simulations for lower number of degrees of freedom. Its accuracy improves with increasing number of degrees of freedom consistent with the *h*-refinement method in literature. Notably, the standard ten-node element performs well for D-type

and C-type structured meshes. This can be attributed to the fact that these discretizations can confine volumetric locking effects within element domains and, in some cases, even cancel these effects between neighboring elements, as documented in [13]. However, it is difficult to generate D-type and C-type meshes for complex geometries. Therefore, unstructured R-type meshes provide more realistic results. The Cosserat point and the modified formulations yield similar results overall; however, as illustrated in Figure 4, the modified ten-node tetrahedra demonstrates better accuracy, except the coarse mesh regime of the S-Type discretization, which is still comparable to the Cosserat point element. The triaxiality contour plots for the coarsest and the finest unstructured R-Type meshes for all three formulations are given in Figure 5, demonstrating the accuracy differences of three element formulations.

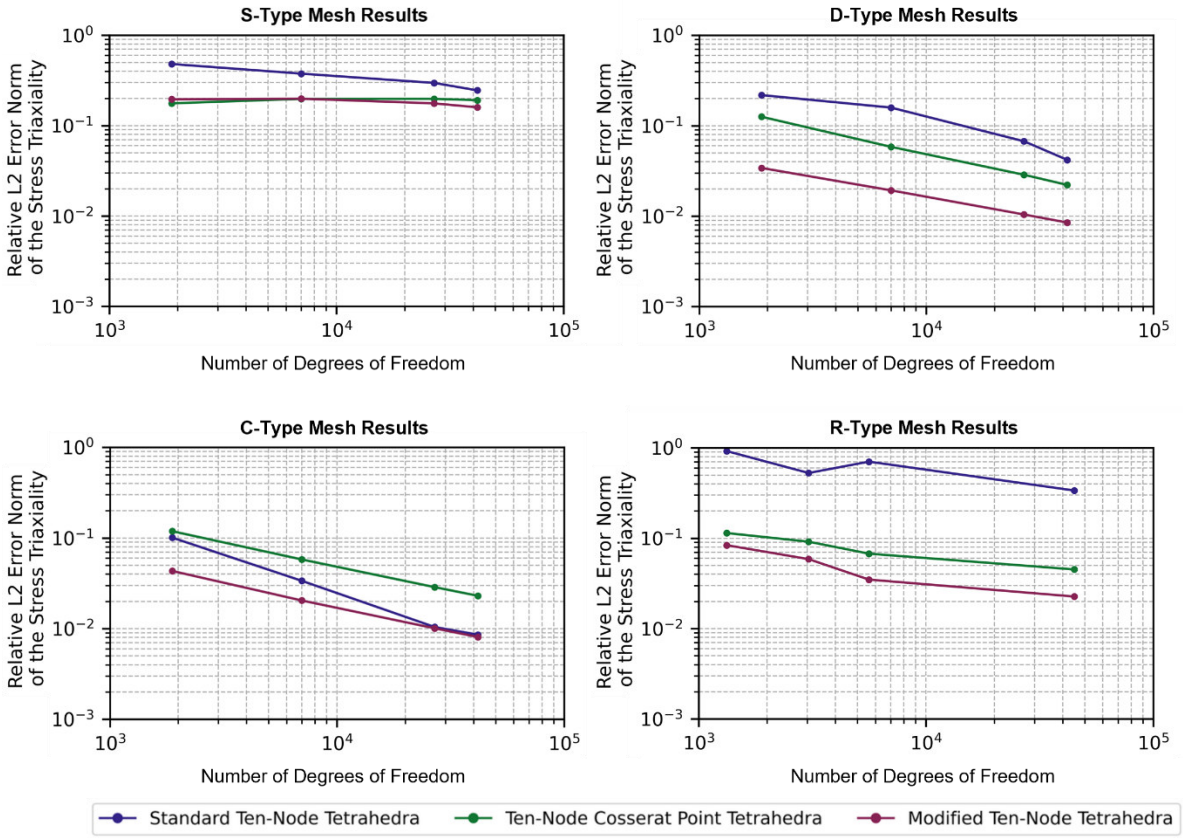

Fig.4: Log-log scale plots for comparing three ten-node tetrahedral element formulations using different finite element discretizations.

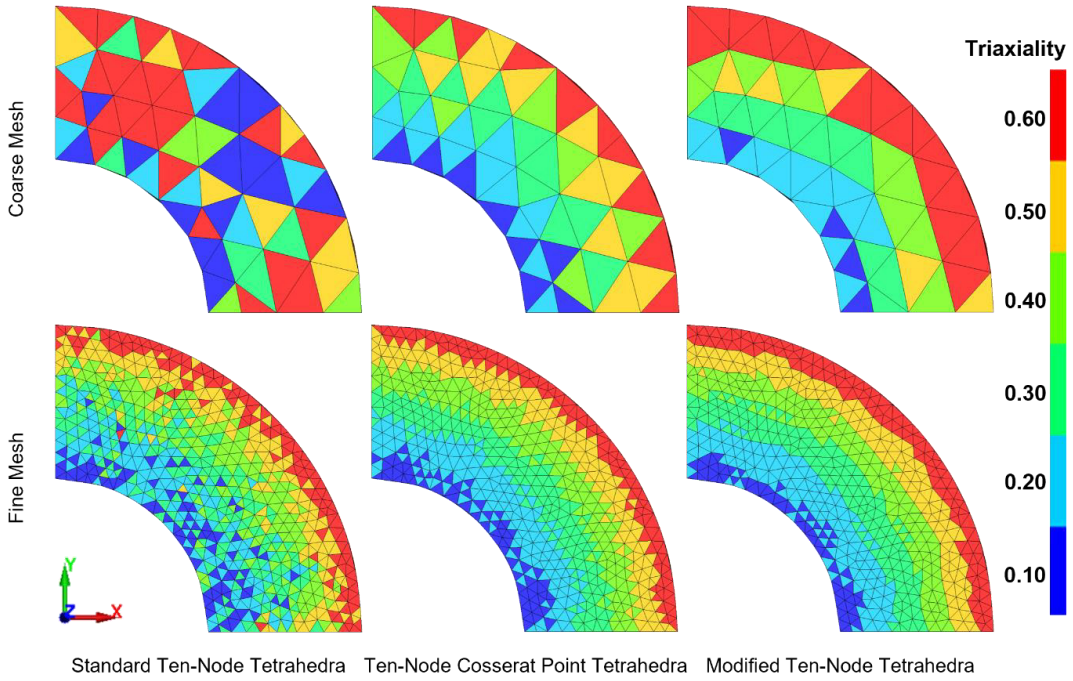

Fig.5: Triaxiality contour plots for the coarsest and finest unstructured R-Type meshes for all three formulations.

5.3 Flat Punch

The flat punch example is adapted from [14] and considered here in the form of a cube, modeled as an explicit quasi-static analysis. The original two-dimensional setup and its three-dimensional extension are illustrated in Figure 6, together with the applied boundary conditions. A uniform prescribed central displacement, $\Delta u = 0.03$, covering one nineth of the total undeformed top surface, is applied on the top surface of the cube. The outer surfaces are constrained in normal direction but remain free to move tangentially. For simplicity, only a quarter of the cube is modeled using a structured mesh consists of 8,748 ten-node tetrahedral elements. The mesh has 40,071 degrees of freedom in total.

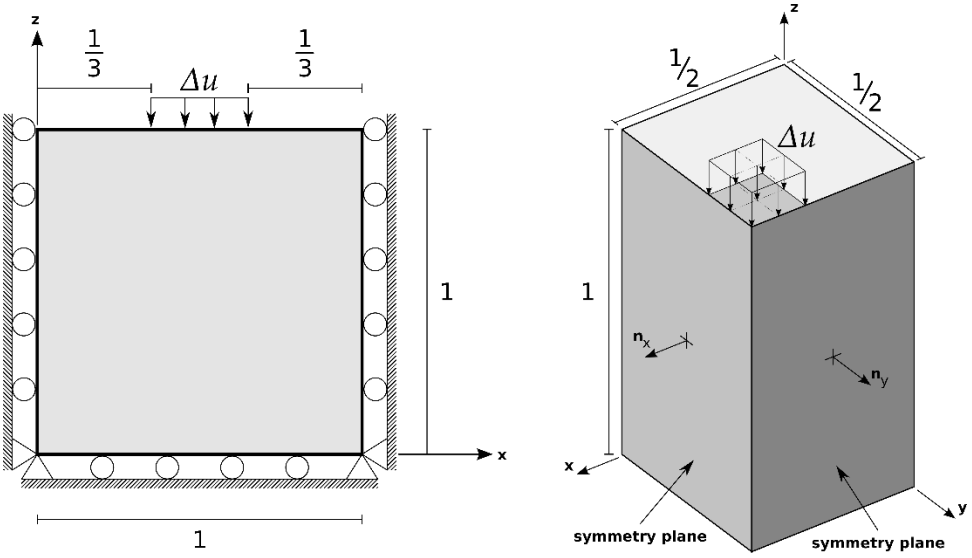

Fig.6: The original flat punch example (left) and a quarter of its three-dimensional variation (right)

The flat punch example was simulated using three formulations: the standard ten-node tetrahedral element, the ten-node Cosserat point tetrahedral element and the proposed modified ten-node tetrahedral element formulation. The pressure field was evaluated, and the results of these formulations are depicted in Figure 7. Both results for the Cosserat point element and the modified element show consistent and smooth pressure fields, while the result for the standard tetrahedra exhibited pronounced oscillations in the pressure field, which is an indicator for the volumetric locking.

Focusing on the Cosserat point element and the modified element, the pressure field contour plots were extracted along a cross-sectional plane from the center of the cube to an outer corner across the full cube height. The results indicate that the modified element provides a more accurate pressure distribution compared to the Cosserat point element, as illustrated in Figure 8. Moreover, in terms of the computational time, the modified ten-node tetrahedra requires only about one third of the total simulation time of the Cosserat point tetrahedra.

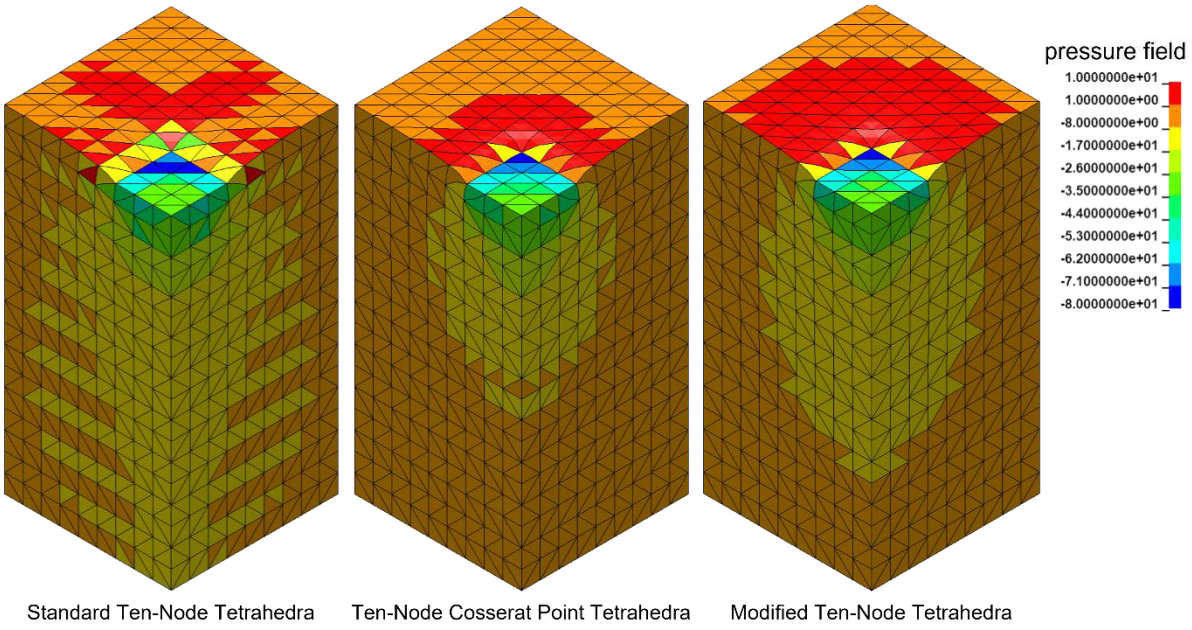

Fig.7: Pressure field results of the flat punch example using various tetrahedral element formulations

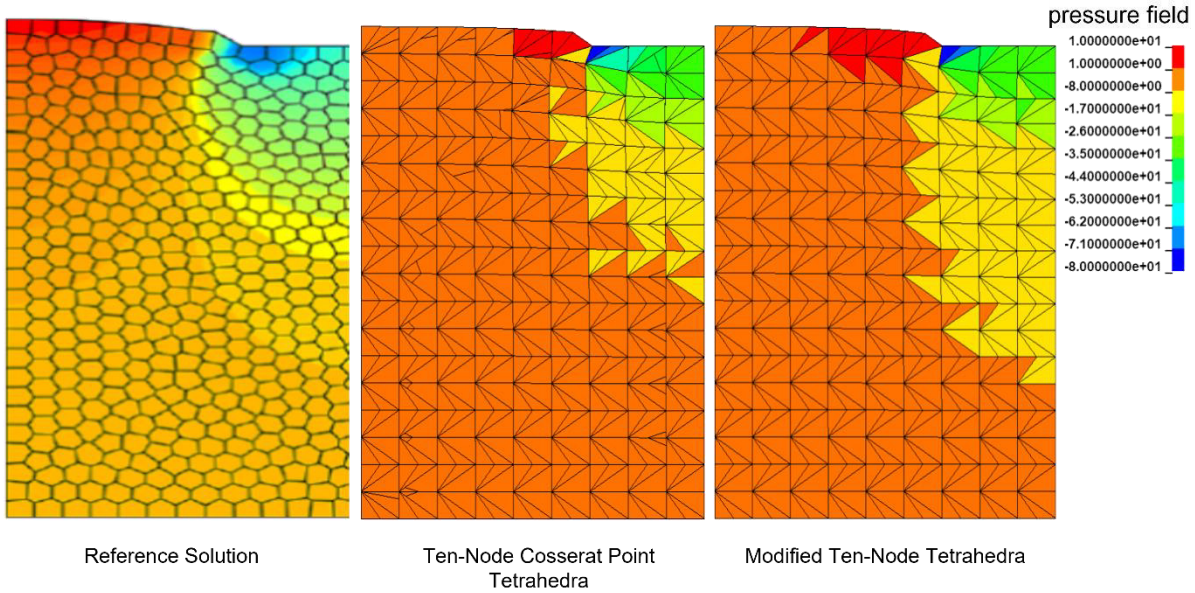

Fig.8: Reference pressure field solution [14] and FEM results along a diagonal cross-section through the total height of the cube for Cosserat point tetrahedra and modified tetrahedra

6 Conclusion

In this work, a modified ten-node tetrahedral element formulation has been proposed and evaluated for nearly incompressible isotropic linear elastic material. The formulation is based on splitting the element stiffness matrix into 1 constant and 1 higher-order part, followed by a selective modification of the higher-order contribution. This strategy preserves the element consistency while removing volumetric locking. Furthermore, the formulation has been adapted for explicit time integration, where the modification is applied directly at the level of the internal force vector.

A series of numerical examples, including the patch test, the cylindrical pressure vessel and the flat punch example, was employed to evaluate the performance of the proposed formulation against the standard ten-node tetrahedral element and the ten-node Cosserat point tetrahedral element. The results demonstrate that the standard formulation suffers from severe volumetric locking especially in unstructured meshes, whereas both the Cosserat point and the modified formulations exhibit good accuracy. Notably, the proposed modified formulation achieves comparable or superior accuracy to the Cosserat point formulation while requiring significantly less computational cost. It should also be emphasized that the Cosserat formulation is fundamentally derived by modeling the deformation modes of the element through a strain energy function based on the hyperelastic constitutive equations of the Cosserat point element.

Overall, the proposed element offers a robust and efficient alternative for simulations involving nearly incompressible materials. Its ability to combine accuracy, stability, and computational efficiency makes it a promising candidate for large-scale engineering applications where tetrahedral discretizations are inevitable due to geometric complexity. Future work may focus on extending this approach to nonlinear material behavior.

7 Acknowledgement

We gratefully acknowledge the support for this research from the DigiTain project (19S22006K), funded by the Federal Ministry of Economic Affairs and Energy (BMWE), following on a resolution of the German Bundestag.

8 Literature

[1] Lo, S.H., Ling, C.: “Improvement on the 10-Node Tetrahedral Element for Three-Dimensional Problems”. Computer Methods in Applied Mechanics and Engineering 189, no. 3 (2000): 961–974. https://doi.org/10.1016/S0045-7825(99)00410-7.

[2] Shimada, K.: “Current Trends and Issues in Automatic Mesh Generation”. Computer-Aided Design and Applications 3, no. 6 (2006): 741–750. https://doi.org/10.1080/16864360.2006.10738427.

[3] Bonet, J., Bhargava, P.: “A Uniform Deformation Gradient Hexahedron Element with Artificial Hourglass Control”. International Journal for Numerical Methods in Engineering 38, no. 16 (1995): 2809–2828. https://doi.org/10.1002/nme.1620381608.

[4] Pawlak, T. P., Yunus, S. M., Cook, R. D.: “Solid Elements with Rotational Degrees of Freedom: Part II—Tetrahedron Elements”. International Journal for Numerical Methods in Engineering 31, no. 3 (1991): 593–610. https://doi.org/10.1002/nme.1620310311.

[5] Bonet, J., Burton, A. J.: “A Simple Average Nodal Pressure Tetrahedral Element for Incompressible and Nearly Incompressible Dynamic Explicit Applications”. Communications in Numerical Methods in Engineering 14, no. 5 (1998): 437–449. https://doi.org/10.1002/(SICI)1099-0887(199805)14:5<437::AID-CNM162>3.0.CO;2-W.

[6] Thoutireddy, P., Molinari, J. F., Repetto, E. A., Ortiz, M.: “Tetrahedral Composite Finite Elements”. International Journal for Numerical Methods in Engineering 53, no. 6 (2002): 1337–1351. https://doi.org/10.1002/nme.337.

[7] Pakravan, A., Krysl, P.: “Mean-strain 10-node Tetrahedron with Energy-sampling Stabilization for Nonlinear Deformation”. International Journal for Numerical Methods in Engineering 111, no. 7 (2017): 603–623. https://doi.org/10.1002/nme.5473.

[8] Jabareen, M., Hanukah, E., Rubin, M. B.: “A Ten Node Tetrahedral Cosserat Point Element (CPE) for Nonlinear Isotropic Elastic Materials”. Computational Mechanics 52, no. 2 (2013): 257–285. https://doi.org/10.1007/s00466-012-0811-x.

[9] Borrvall, T., Rubin, M. B., Jabareen, M.: “Cosserat Point Elements in LS-DYNA”, LS-DYNA Forum, Stuttgart, 2013

[10] Zienkiewicz, O. C., Morice, P. B.: “The finite element method in engineering science”, (Vol. 1977). London: McGraw-hill.123-125.

[11] Belytschko, T., Wong, B. L., Chiang, H.: “Advances in One-Point Quadrature Shell Elements”. Computer Methods in Applied Mechanics and Engineering 96, no. 1 (1992): 93–107. https://doi.org/10.1016/0045-7825(92)90100-X.

[12] Slaughter, W. S.: “The Linearized Theory of Elasticity”. Boston, MA: Birkhäuser Boston, 2002, pp. 263-267, https://doi.org/10.1007/978-1-4612-0093-2.

[13] Ainsworth, M., Parker, C.: “Unlocking the Secrets of Locking: Finite Element Analysis in Planar Linear Elasticity”. Computer Methods in Applied Mechanics and Engineering 395 (2022): 115034. https://doi.org/10.1016/j.cma.2022.115034.

[14] Park, K., Chi, H., Paulino, G. H.: “B-Bar Virtual Element Method for Nearly Incompressible and Compressible Materials”. Meccanica 56, no. 6 (2021): 1423–1439. https://doi.org/10.1007/s11012-020-01218-x.

[15] McCaslin, S. E.: "Closed-form Development of a Family of Higher Order Tetrahedral Elements Through the Fourth Order" (2008). *Mechanical and Aerospace Engineering Dissertations*. 66. https://mavmatrix.uta.edu/mechaerospace_dissertations/66